Structural and electronic properties of glassy $GeSe_2$ surfaces

Xiaodong Zhang and D. A. Drabold
Department of Physics and Astronomy, Condensed Matter and Surface Science Program, Ohio University, Athens, Ohio 45701
(Received 6 June 2000)

We report first-principles structural models of surfaces of glassy $GeSe_2$ (g-$GeSe_2$). The structural properties of bulk and surface g-$GeSe_2$ are compared with recent experimental data. The first diffraction peaks in the partial structure factors are accurately reproduced in both the surface and bulk models. We also examine the transition of the local bonding environment from the bulk to the surface. The surface reconstruction involves creation of several edge-sharing tetrahedra and electronic states are easily delocalized through rings formed in the reconstruction.

I. INTRODUCTION

Amorphous Ge-Se semiconductors have potential applications for optical storage devices, solar cells, and other devices, that require materials which are photosensitive.[1] As a classic glass-former g-$GeSe_2$ has been intensely studied.[2–6] The material has been thoroughly reviewed by Boolchand[7] and applications of this and related glasses are discussed by Ovshinsky.[8]

One of the principal remaining puzzles for bulk $GeSe_2$ glass is the nature of the celebrated ''first sharp diffraction peak'' (FSDP) which is often interpreted as arising from *some* type of ordering on an intermediate range ($\sim 6-10$ Å) scale. In experiments on liquid[9] $GeSe_2$ and glassy[6] $GeSe_2$ it was demonstrated that a FSDP also occurred in the Bhatia-Thornton[10] concentration-concentration partial structure factor S_{CC}. However, some molecular dynamics simulations[3,5] did not yield concentration fluctuations in liquid $GeSe_2$. Massobrio *et al.*[5] have argued that gradient corrections (generalized gradient approximation) to the local density approximation (LDA) of density functional theory are required to get a FSDP even in the total structure factor. More recently these authors suggested that a simple effect of increased ionicity (a by-product of using a larger number of plane waves) was required to obtain a weak FSDP in S_{CC} for l-$GeSe_2$ using plane wave methods.[11] We explicitly demonstrate here by direct comparison to recent experiments[6] that the FSDP *and other experimental attributes of* g-$GeSe_2$ are well reproduced by a 216-atom model[4] computed with the Harris functional LDA as described below.

Little is known about the structural and electronic properties of g-$GeSe_2$ surfaces. We propose atomistic models of these surfaces which are interesting both in their own right and also, to our knowledge as the first *ab initio* model of the surface of a glass. The nature of the ''surface reconstruction'' for a binary glass is elucidated and it is found to proceed largely by ring formation. Atomic force microscopy (AFM) has some potential to attack the unresolved questions about the atomic surface structure of amorphous insulators although currently not with atomic-level resolution. We will show here that there are clear manifestations of the bulk structure including even a FSDP, from the first few surface layers.

The rest of this paper is organized as follows. In Sec. II we discuss the computational methodology of the study; in Sec. III we discuss the models obtained and compare them to experiment. in Secs. IV and V the electronic properties of the surfaces are discussed with some emphasis on the metal-insulator (Anderson) transition and the interplay between bulk and surface localized electron states.

II. PRELIMINARY THEORETICAL CONSIDERATIONS

Structural calculations for the surface model have been performed with a local orbital first-principles quantum molecular dynamics method designed for application to large complex systems.[12] The method employs density functional theory within the local density approximation and hard norm-conserving pseudopotentials. The method is entirely real space (except for a simple Ewald summation). The short-range nonorthogonal single-ζ local orbital basis of the compact slightly excited ''fireball'' orbitals of Sankey and Niklweski offers an accurate description of the chemistry with a significant computational advantage,[13] ideal for this complex material. Applications of the technique to several materials problems are reviewed in Refs. 14 and 15.

Using this method Cobb, Drabold, and Cappelletti[4] constructed a 216-atom bulk g-$GeSe_2$ model that correctly reproduced the first sharp diffraction peak around 0.91 Å. The total structure factor, vibrational density of states, dynamical structure factor, and electronic density of states were in good agreement with experimental data. This work also revealed that defective threefold Ge atoms were correlated with onefold Se atoms at a distance of about 3.2 Å, suggesting that the threefold Ge atoms are mostly defective $Ge(Se_{1/2})_4$ tetrahedra. This weaker correlation between defective Ge and Se was recently confirmed by experiment.[6] Satisfactory agreement with several independent measurements recommends the bulk model and Hamiltonian as suitable for studies of the surface.

To construct a model of the surface we initially break the periodicity along the z direction to transform the periodically extended cube into an infinite slab with two free surfaces (one labeled as the ''top'' and the other as the ''bottom''). Then the slab is relaxed with our molecular dynamics code to search for the the new minimal energy configuration with the slab geometry.

After the periodic boundary condition along the z axis is

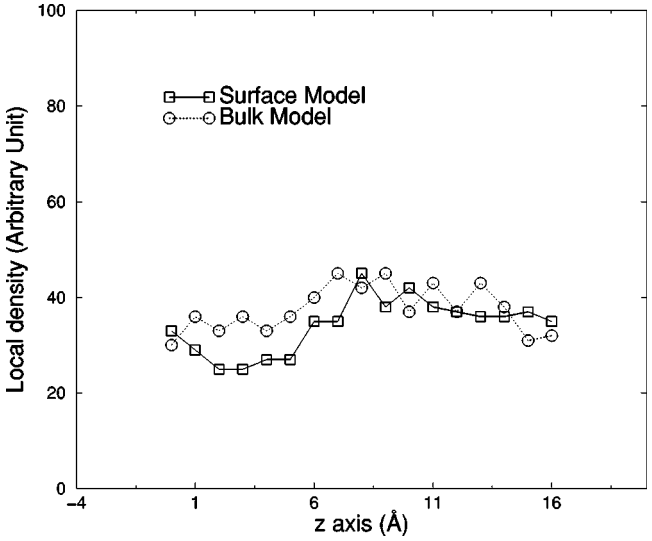

FIG. 1. Local density (averaged over at a 3 Å thickness) at different depths of bulk and surface models of g-$GeSe_2$.

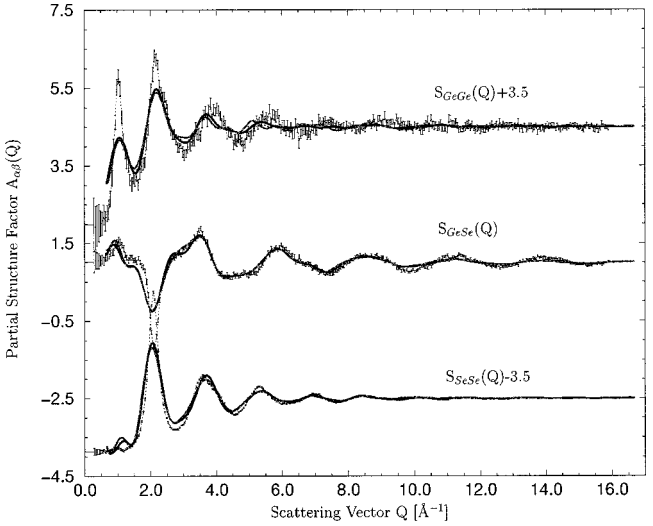

FIG. 2. The calculated partial structure factors $A_{\alpha\beta}(Q)$ for g-$GeSe_2$ compared to experimental data from Ref. 6. The black line and gray line are calculated data for bulk model and slab model, respectively.

broken, dangling bonds will appear on the surface. Structural relaxation will lead to some major local bonding rearrangements near the surfaces. The total energy of our slab model is about 0.15 eV/atom lower than that of the unreconstructed g-$GeSe_2$ model. Initially, at the bulk density our slab models expand slightly along the normal direction of the surface during the relaxation. In Fig. 1 we show the local density (averaged in a neighborhood of 3 Å) at different depths of the bulk model and surface model. Our slab model is nearly as homogeneous as the bulk phase with only a small local density fluctuation.

III. STRUCTURE FROM QUANTUM MOLECULAR DYNAMICS

In this section we present a rather detailed comparison of our earlier bulk model[4] to very recent experiments and discuss the structure of the slab models obtained from the preceding section. The structure of these models is analyzed through partial Faber-Ziman structure factors. The Faber-Ziman structure factors are defined as:

$$A_{\alpha\beta}=1+4\pi\rho\int[g_{\alpha\beta}(r)-1]\,\frac{\sin(Qr)}{Qr}r^2dr, \qquad (1)$$

where ρ is the number density of the system and

$$g_{\alpha\beta}(r)=\frac{1}{4\pi r^2\rho N c_\alpha c_\beta}\sum_{i\neq j}\delta(r-r_{ij}). \qquad (2)$$

Here c_α denotes the fraction of species α in the total system. The Bhatia-Thornton partial structure factors are defined as:

$$\begin{aligned} S_{NN}&=c_1^2A_{11}+c_2^2A_{22}+2c_1c_2A_{12}\\ S_{NC}&=c_1c_2[c_1(A_{11}-A_{12})-c_2(A_{22}-A_{12})], \qquad (3)\\ S_{CC}&=c_1c_2[1+c_1c_2(A_{11}+A_{22}-2A_{12})], \end{aligned}$$

that is, they are concentration-weighted combinations of the Faber-Ziman structure factors.

Figure 2 shows the calculated Faber-Ziman partial structure factors for our bulk and slab models. The calculated results show pleasing agreement with (bulk) experiment for both bulk model and surface model. The first sharp diffraction peak at $Q=1.00$ Å^{-1} arises predominantly from the Ge-Ge correlations. The intensity differences for $Q<3$Å^{-1} is a finite size artifact.[16]

In Fig. 3 the calculated Bhatia-Thornton structure factors are compared with experimental data. The number-number structure factor S_{NN} resembles the total structure factor since the scattering lengths of Se and Ge are very close. So our bulk model and surface model describe the experimental total structure factor rather well. Most molecular dynamics investigations fail to reproduce the concentration-concentration partial structure factor S_{CC} (in liquid $GeSe_2$).[5,3] In our bulk and surface model we clearly observe the FSDP feature in S_{CC}.

Some characteristics of surface reconstruction can be seen from the partial pair correlation functions for both surface model and bulk models. (Fig. 4). As in the bulk phase, the Ge-Se bond length of 2.37 Å is quite close to the crystal Ge-Se bond length of 2.355 Å. There are still Ge-Ge and Se-Se bonds. A significant feature of the slab model is the strong enhancement at 3.05 Å in the Ge-Ge correlation function. The 3.05 Å peak in $g_{\text{Ge-Ge}}$ is due to correlation between edge-sharing tetrahedra. The increase of the strength of this peak in the slab model indicates that the surface atoms of g-$GeSe_2$ are reconstructed in part through forming edge-sharing tetrahedra. The fraction of edge-sharing Ge atoms in the bulk model is 47%, which is close to experimental values of 40%,[17] and 35(5)%.[6] However, this increases to 69% in the slab surface model. Vashishta *et al.*[18] found that there was significant improvement in the FSDP as the fraction of edge-sharing tetrahedra increased. Our previous study[4] also indicated that the FSDP had a strong dependence on the fraction of edge-sharing tetrahedra.

The surface reconstruction of the g-$GeSe_2$ model can be seen more clearly from the microstructure of the surface lay-

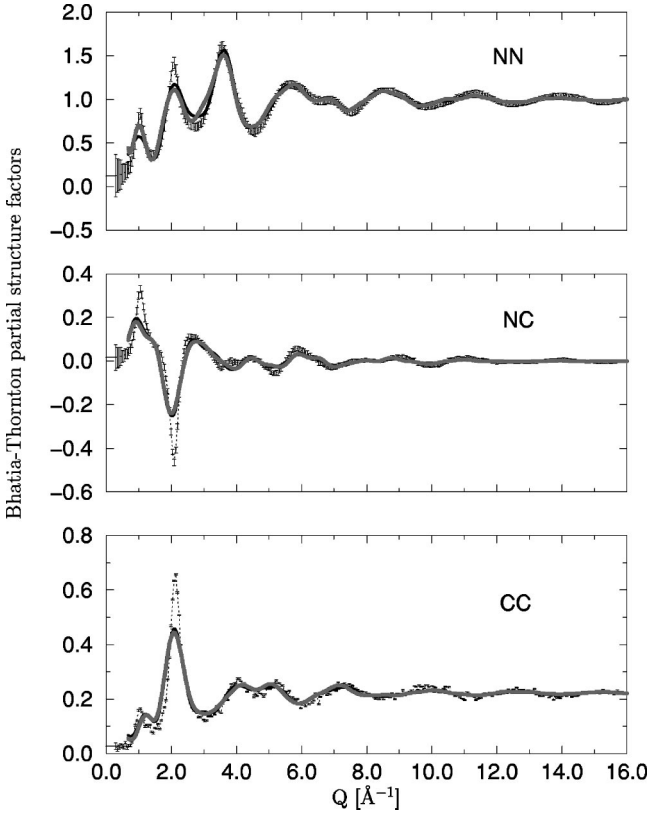

FIG. 3. The Bhatia-Thornton partial structure factors for g-$GeSe_2$ compared to experimental data from Ref. 6. The black line and gray line are calculated data for bulk model and slab model, respectively.

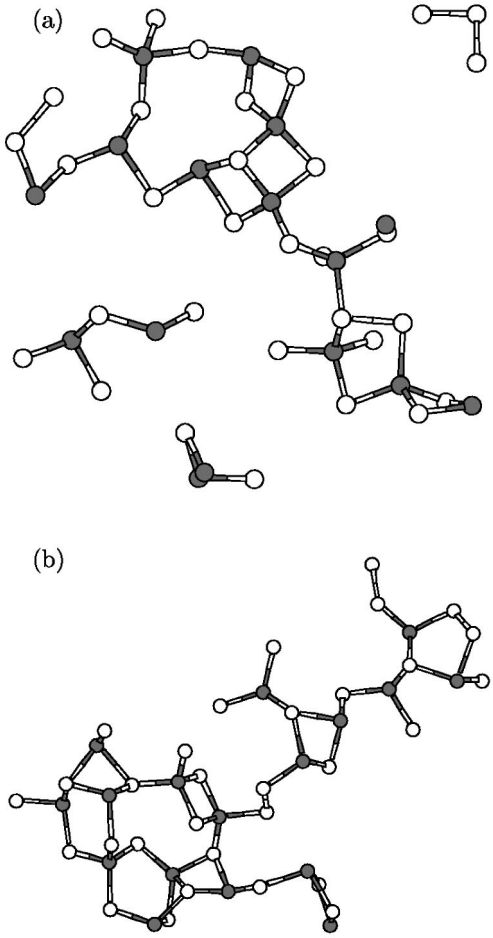

FIG. 5. The microscopic structure of the top (a) and bottom (b) surfaces for the slab model. The dark color indicates the Ge atoms and white represents Se atoms. The periodic boundary conditions are imposed in the plane of the figures.

ers. To focus on the surface character of our slab model we choose the 50 atoms closest to vacuum above (or below) as the top (or bottom) surface. Figure 5 shows the surface structure of our slab model. There is a clear tendency for ring formation at both surfaces. Earlier Dong and Drabold[19] studied the surface reconstruction of ta-C (tetrahedral amorphous carbon). They found that planar ring or chain formation was the dominant surface reconstruction mechanism. It is quite interesting that for a binary amorphous material like g-$GeSe_2$ the atoms at the surface still reconstruct through ring formation. The enhancement of ring formation can be seen explicitly through the ring statistics.

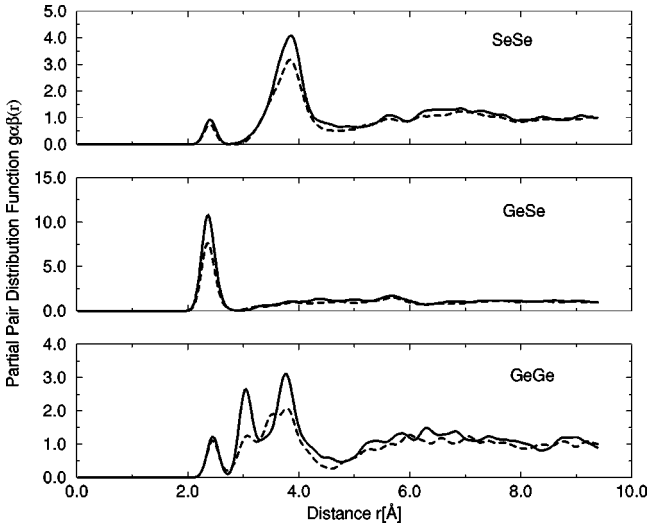

FIG. 4. The partial pair correlation functions for bulk g-$GeSe_2$ and slab g-$GeSe_2$. The dashed line and solid line are calculated data for the bulk model and slab model, respectively.

From Table I we can see that the number of four-, eight-, and ten-member rings exhibits a major increase indicating that more edge-sharing tetrahedra are formed during the surface reconstruction. This can be intuitively understood by the fact that a ring is a relatively planar structure and it is a very reasonable structure to enable the atoms to maintain their preferred coordination at a surface.

The statistics of the number of atoms of each type of coordination for the slab model and bulk model is listed in Table II. An interesting feature is that the fractions of three- and four-coordinated Ge atoms are similar in the bulk and

TABLE I. Ring statistics: the number of n-order rings ($n=3-11$) for bulk and surface $GeSe_2$ models.

Ring size	3	4	5	6	7	8	9	10	11
Bulk	3	20	10	23	3	12	7	9	20
Surface	5	27	10	25	6	20	9	27	26

TABLE II. Coordination number distribution in the slab model and bulk model. The number in parentheses denotes the percentage of the atoms in this configuration. For the bulk model there is a five-coordinated Ge atom that is not listed in the table.

		No. of atoms		
Atom	Coordination	Surface only	Whole slab	Bulk
Se	1	12(12%)	18(8%)	15(7%)
	2	36(36%)	92(43%)	101(47%)
	3	20(20%)	33(15%)	28(14%)
Ge	3	10(10%)	13(6%)	13(6%)
	4	22(22%)	59(27%)	58(27%)

surface models. However, undercoordinated Ge atoms segregate in the surface layer. This suggests that some undercoordinated Ge atoms in the bulk region become ideally (four-) coordinated Ge atoms during surface reconstruction. This result shows that the ''sp^2'' concentration will be higher in the surface region. Experimental results on the ta-C surface confirmed higher sp^2 content in the surface region.[20]

The first sharp diffraction peak observed in g-$GeSe_2$ is often interpreted as a consequence of ordering on an appropriate intermediate length scale. However what structure with intermediate order governs the FSDP has not been determined with certain. The difficulty in determining the microscopic origin of the FDSP originates from the fact that no experiment can measure the structure in sufficient detail. Figure 6 shows the surface-projected Bhatia-Thornton partial structure factors. This surface was formed by choosing the 70 atoms closest to vacuum. The thickness of this surface is about 6.5 Å. The S_{NN} structure factor of this surface region almost reproduces the S_{NN} of the whole slab model but the FSDP in S_{CC} was not seen from this slab. Thus to a significant degree, the 70 surface atoms carry the overall structural information of the entire $GeSe_2$ model. This result indicates that it may be possible to determine the origin of the FSDP experimentally by studying the microscopic structure of the surface atoms. We hope future AFM experiments can confirm this conjecture.

IV. ELECTRONIC PROPERTIES

The electronic properties of our slab model are analyzed through the electronic density of states and inverse participation ratio. A point of interest in this section is the nature of localized ''surface states'' for an amorphous material. Their formation of ''surface bands'' and resonant mixing with bulk defects are interesting features of this study.

For both the slab and bulk models we did not see an obvious change of electronic density of states. Although there are more defects in the slab model compared to the bulk model the Γ-point band gap in the slab model is 1.61 eV, which is only slightly smaller than the gap of 1.72 eV in the bulk model. There are still no states in the fundamental band gap despite the overall increase in defects for the slab. To connect localized eigenstates to particular topological/chemical irregularities we compute the inverse participation ratio

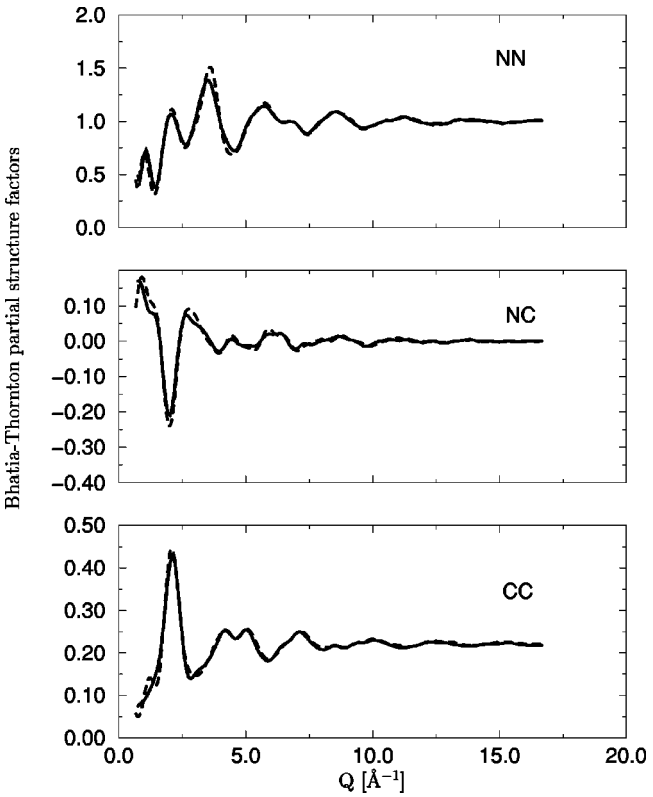

FIG. 6. The surface-projected Bhatia-Thornton partial structure factors for the slab model. The dashed line and solid line are the Bhatia-Thornton partial structure factors for the whole slab and the surface region, respectively. The surface region was defined as the 70 atoms closest to vacuum for the bottom surface of the slab model.

$$Q_2(E) = N \sum_{n=1}^{N} q(n,E)^2, \tag{4}$$

where N is the number of atoms in the slab model and $q(nE)$ is the Mulliken charge[22] localized on atomic site n in a certain eigenstate E. A larger $Q_2(E)$ means that the eigenstate is more localized in real space and the individual contributions to the sum indicate which sites are most responsible for the localization. Figure 7 shows the individual electronic eigenstates near the band gap for both slab model and bulk model. In the slab model there are more localized states near the valence band and conduction band edges.

By examining the localized states at the band edges we found that the localized states at the valence band edge derive mostly from undercoordinated Ge atoms and one-coordinated Se atoms. The localized states at the conduction band edge are mostly due to three-coordinated Se atoms. The defect states in the slab model reveal that the valence alternation pair model, which explains most electronic properties of elemental amorphous Se,[21,23,24] still plays an important role in this binary chalcogenide glass. But in the g-$GeSe_2$ model the undercoordinated Ge atoms and one-coordinated Se atoms together served as the C^- center and the three-coordinated Se atoms play the role of the C^+ center. Compared to the bulk model, many localized states in the slab model exhibit surface character. Table III lists the localization and defect type for the atoms at the conduction band edge and valence band edge.

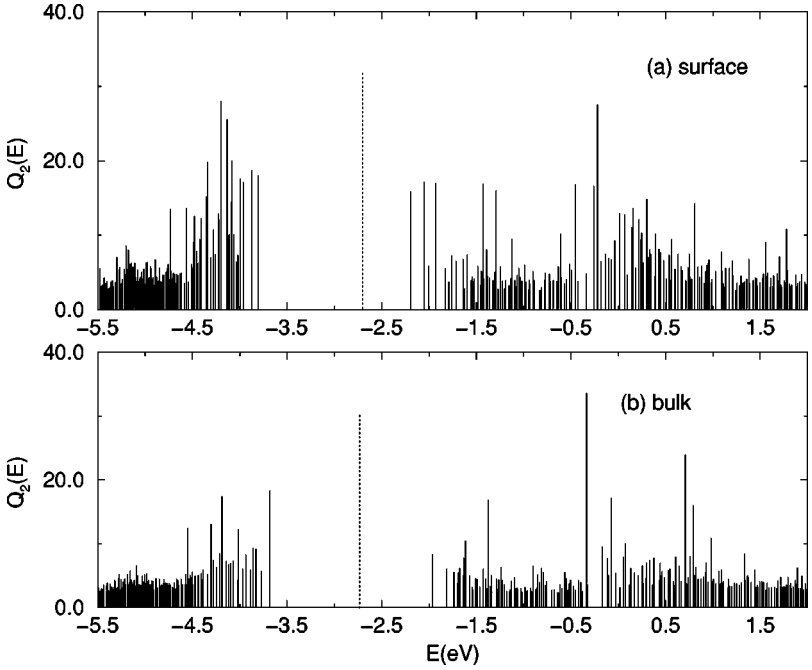

FIG. 7. Inverse participation ratio in the band gap region for the slab model and bulk model. The vertical dotted indicates the position of the Fermi level.

From Table III we can see that the localization of electronic states near the band edge derives mostly from surface atoms. Some strained ideally coordinated atoms and defective atoms make a contribution to the localization of electronic states. If we take a close look at the atoms that contribute to localization, we observe that most of these are connected with some defect sites. For example, a Se atom (number 185) with strong localization is very close to the undercoordinated Ge atom (number 211). Ge (number 9) contributes to the localization at the conduction band edge and is a neighbor of the three-coordinated Se atom (number 34). Thus we infer that undercoordinated Ge and Se atoms lead to the localized states at the valence band edge and overcoordinated Se atoms cause the localization at the conduction band edge. This seems to confirm the valence alternation model of Kastner *et al.*[21]

For a tetrahedral amorphous carbon surface and a 4096-atom a-Si model,[25] Dong and Drabold found that the spatial character of the eigenstates from the Fermi level into the interior of the valence states goes through an Anderson (localized-to-extended) transition. We find a qualitatively similar transition in this binary glass.

To examine the atomistic spatial structure of the electronic eigenstate we use the same visualization scheme as Dong and Drabold.[25] The basic procedure is as follows. For a given electronic eigenstate we compute the electron charge associated with each atom. Each atom is drawn in one of four levels of the gray scale according to the amount of charge associated with it (Fig. 8). Black atoms depict strong localization centers that contribute more than 10% of the total charge each, less dark atoms are sites that contribute more than 2.5%, each light atoms are sites that contribute

TABLE III. The coordination and localization of atoms at the conduction band edge and valence band edge. Region 1 indicates the top and bottom surface regions and region 2 indicates the bulk region.

	Valence band edge				Conduction band edge			
Region	Atom	E(eV)	$q(n,E)$	Coord.	Atom	E(eV)	$q(n,E)$	Coord.
1	3(Se)	−4.73	7.3	1	9(Ge)	−0.46	6.80	4
	18(Se)	−4.42	5.74	1	10(Ge)	0.24	7.40	3
	21(Se)	−3.96	6.31	1	23(Se)	−0.21	19.03	3
	25(Ge)	−3.99	6.72	3	25(Ge)	0.23	6.15	3
	185(Se)	−4.77	7.17	2	29(Ge)	0.16	6.11	3
	198(Ge)	−4.20	12.83	3	31(Se)	−1.43	8.30	3
	210(Se)	−4.08	6.06	2	34(Se)	−1.43	7.29	3
	211(Ge)	−4.08	6.11	3	47(Se)	−1.93	6.50	3
	213(Ge)	−4.13	8.52	3	193(Ge)	−0.26	8.54	3
	215(Se)	−4.13	10.61	1				
2	69(Ge)	−3.87	8.67	3	69(Ge)	0.80	9.48	3
	76(Se)	−4.56	7.67	1	63(Se)	−1.93	5.61	2
	112(Ge)	−3.80	8.33	4				
	133(Se)	−4.33	13.65	2				
	164(Se)	−4.35	7.76	2				

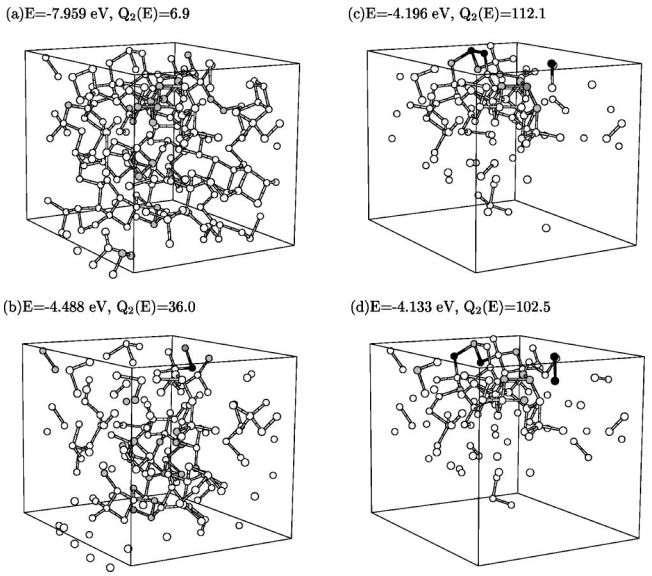

FIG. 8. Spatial character of the bulk-to-surface transition of valence electronic states in the surface slab model. The electronic states evolve from (a) bulklike extended states in the middle of the valence band to (b) less extended states to (c) more surfacelike states to (d) surfacelike localized states. The color is coded according to the fraction of total charge: black ($\geqslant$10%), less dark ($\geqslant$2.5%), light ($\geqslant$1%), and white ($\leqslant$1%). Only 99% of the total charge is shown.

more than 1% each, and white atoms contribute the rest. For clarity, 99% of the total charge is present and those atoms that contribute the remaining 1% charge for the given eigenstates are omitted in the figure.

We can see from Fig. 8 that the extended-to-localized transition (for energies ranging from midband to midgap) of electronic eigenstates proceeds from the bulk-to-surface transition on the g-$GeSe_2$ surface. In our slab model the states from inside the valence band are bulklike extended states. In this region [Fig. 8(a)] we did not observe any significant charge localization caused by surface atoms. When we approach an energy near -4.5 eV the surface localized defect begins to be manifested in the charge localization [Fig. 8(b)]. However, the states are still quite extended. When the energy approaches -4.2 eV [Fig. 8(c)] the influence from surface atoms becomes dominant. Figure 8(d) shows strongly localized surface states and most charges are localized at the surface region.

V. DEFECTS AND CHARGE LOCALIZATION

For both slab model and bulk model there are many defect sites. However, we did not observe any states in the fundamental band gap. Our model also correctly reproduces the FSDP in the structure factor with a fairly large number of defect sites. It is important to know how the defect sites manifest themselves in the electronic eigenstates. Figure 9 shows the inverse participation ratio for the whole energy range and typical defect structures causing the localization of eigenstates. The localized states at -18.4 eV, -8.8 eV, and -13.7 eV are due to overcoordinated Se influenced by an undercoordinated Ge atom [defect type (a) in the right panel of Fig. 9]. The localized states around -15.7 eV to -14.7 eV are mainly due to undercoordinated Se atoms [defect type (b)], Se-Se wrong bonds [defect type (c)], and overcoordinated Se atoms [defect type (a)]. The state at -12.43 eV is caused by Ge-Ge wrong bonds [defect type (d)]. The localization at the top of valence band is caused by a ring structure consisting of two undercoordinated Ge atoms, one onefold Se atom, and one threefold Se atom [defect type (e)]. We notice that this state is not as localized as defect types (a), (b), (c), and (g). The localiza-

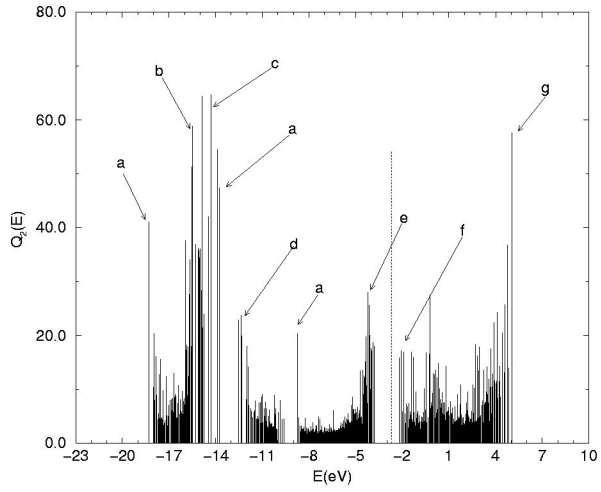

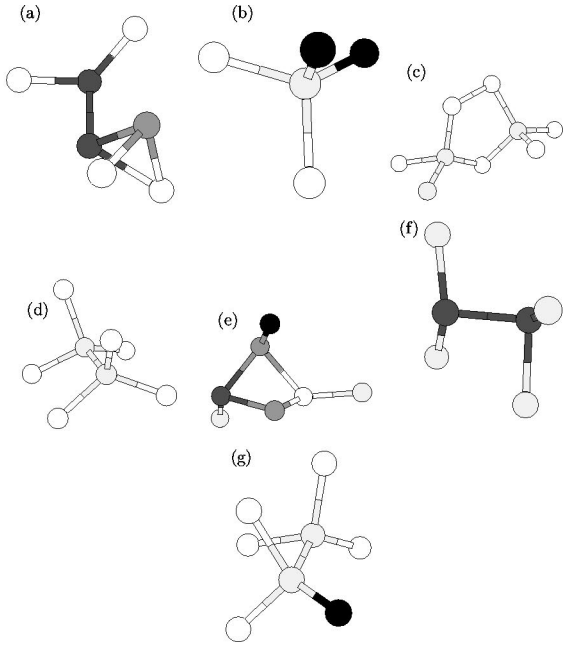

FIG. 9. The characteristic defect types causing localization in the electronic eigenstates in the slab model. The defects are visualized as onefold Se atoms (black), threefold Se atoms (less dark), threefold Ge atoms (gray), fourfold Ge atoms (light gray), and two fold Se atoms (white). The vertical dotted line indicates the position of the Fermi level.

tion at the bottom of the conduction band is caused by overcoordinated Se atoms [defect type (f)]. The state at 5.02 eV derives from a Ge-Ge wrong bond influenced by onefold Se atoms. The most defective structures do not cause localized states in the fundamental band gap but make some localized states far inside the valence band and conduction band. At the band edge the defect-defect interaction makes the electronic eigenstates less localized. This kind of delocalization is explained by Dong and Drabold's resonant cluster proliferation model. The delocalization is via clusters with similar electronic energies. The defect types (e) and (f) in our slab $GeSe_2$ model confirmed this resonant tunneling mechanism. This is the reason why defect type (c) with a Se-Se wrong bond causes more localized states than the geometrically more defective structures (e) and (f).

VI. CONCLUSION

We have reported a structural model of g-$GeSe_2$ surfaces constructed by first-principles molecular dynamics simulation. The full partial structure factors are compared with experimental data. In particular, the FSDP feature in the Bhatia-Thornton concentration-concentration partial structure factor S_{CC} was observed. We also find that the FSDP feature emerges at 6.5 Å thickness of the surface closest to vacuum. So it maybe possible to explore the FSDP structure by AFM or perhaps scanning tunneling microscopy (if the material can be made at least weakly conducting). Compared to the bulk g-$GeSe_2$ model, the slab $GeSe_2$ model has more edge-sharing tetrahedra. As in the case of ta-C, planar rings are formed on the surface of the slab model. We also observe that electronic states evolve from bulklike extended states inside the bands to surfacelike localized states in the band tail. The surface localized states can be delocalized through the resonant cluster proliferation mechanism.

ACKNOWLEDGMENTS

We would like to thank Professor P. S. Salmon for providing the data reported in Ref. 6. We acknowledge many helpful conversations with Ron Cappelletti, Punit Boolchand, Normand Mousseau, and Jun Li. This work was performed in part under the auspices of the U.S. NSF under Grant Nos. DMR 96-04921 and DMR-00-81006.

[1] K.M. Kandil *et al.*, Phys. Rev. B **51**, 17 565 (1995).
[2] P. Boolchand and W.J. Bresser, Philos. Mag. B **80**, 1757 (2000); P. Boolchand, J. Grothaus, W.J. Bresser, and P. Suranyi, Phys. Rev. B **25**, 2975 (1982).
[3] P. Vashishta R.K. Kalia, J.P. Rino, and J. Ebbsjö, Phys. Rev. B **41**, 12 197 (1990).
[4] Mark Cobb, D.A. Drabold, and R.L. Cappelletti, Phys. Rev. B **54**, 12 162 (1996).
[5] C. Massobrio, A. Pasquarello, and R. Car, Phys. Rev. Lett. **80**, 2342 (1998).
[6] I. Petri, P.S. Salmon, and H.E. Fischer, Phys. Rev. Lett. **84**, 2413 (2000).
[7] See, for example, P. Boolchand, in *Insulating and Semiconducting Glasses*, edited by P. Boolchand (World Scientific, Singapore, 2000), p. 191, especially Sec. 4.1.
[8] S. Ovshinsky, in *Insulating and Semiconducting Glasses* (Ref. 7), p. 729.
[9] I.T. Penfold and P.S. Salmon, Phys. Rev. Lett. **67**, 97 (1991).
[10] A. Bhatia and D. Thornton Phys. Rev. B **2**, 3004 (1970).
[11] C. Massobrio, A. Pasquarello, and R. Car, Comput. Mater. Sci. **17**, 15 (2000).
[12] A.A. Demkov, J. Ortega, O.F. Sankey, and M.P. Grumbach, Phys. Rev. B **52**, 1618 (1995).
[13] O.F. Sankey and D.J. Niklewski, Phys. Rev. B **40**, 3979 (1989).
[14] O.F. Sankey, A.A. Demkov, W. Windl, J.H. Fritsch, J.P. Lewis, and M. Fuentes-Cabrera, Int. J. Quantum Chem. **69**, 327 (1998).
[15] D. A. Drabold, X. Zhang, and S. Nakhmanson, in *Properties and Applications of Amorphous Materials*, of *NATO Advanced Study Institute, Series B: Physics*, edited by M. F. Thorpe and L. Tichy (Kluwer, Dordrecht, in press).
[16] A. Uhlherr and S.R. Elliott, Philos. Mag. B **71**, 611 (1995); for a recent discussion see, S.R. Elliott, Phys. Rev. Lett. **67**, 711 (1991); Nature (London) **354**, 445 (1991).
[17] S. Susman, K.J. Volin, D.G. Montague, and D.L. Price, J. Non-Cryst. Solids **125**, 168 (1990).
[18] P. Vashishta, R.K. Kalia, G. Antonio, and I. Ebbsjö, Phys. Rev. Lett. **62**, 1651 (1989).
[19] Jianjun Dong and D.A. Drabold, Phys. Rev. B **57**, 15 591 (1998).
[20] C.A. Davis, K.M. Knowles, and G.A.J. Amaratunga, Surf. Coat. Technol. **76-77**, 316 (1995).
[21] M. Kastner, D. Adler, and H. Fritzsche, Phys. Rev. Lett. **37**, 1504 (1976).
[22] A. Szabo and N. S. Ostlund, *Modern Quantum Chemistry* (Dover, New York, 1996).
[23] X. Zhang and D.A. Drabold, Phys. Rev. Lett. **83**, 5042 (1999).
[24] X. Zhang and D.A. Drabold, J. Non-Cryst. Solids **241**, 195 (1998).
[25] J. Dong and D.A. Drabold, Phys. Rev. Lett. **80**, 1928 (1998).